Catalysis Science & Technology

Accepted Manuscript

This is an *Accepted Manuscript*, which has been through the Royal Society of Chemistry peer review process and has been accepted for publication.

Accepted Manuscripts are published online shortly after acceptance, before technical editing, formatting and proof reading. Using this free service, authors can make their results available to the community, in citable form, before we publish the edited article. We will replace this *Accepted Manuscript* with the edited and formatted *Advance Article* as soon as it is available.

You can find more information about *Accepted Manuscripts* in the Information for Authors.

Please note that technical editing may introduce minor changes to the text and/or graphics, which may alter content. The journal's standard Terms & Conditions and the Ethical guidelines still apply. In no event shall the Royal Society of Chemistry be held responsible for any errors or omissions in this *Accepted Manuscript* or any consequences arising from the use of any information it contains.

ROYAL SOCIETY OF CHEMISTRY

www.rsc.org/catalysis

Catalysis Science and Technology

ARTICLE

Catalysis Science & Technology Accepted Manuscript

Cation doping size effect for methane activation on alkaline earth metal doping of the CeO_2 (111) surface

Received 00th January 20xx,
Accepted 00th January 20xx

DOI: 10.1039/x0xx00000x

www.rsc.org/

J. J. Carey,[a†] M. Nolan[a†]

Methane is an extremely important clean fuel source; however, its activation is extremely difficult due to the large energy required to break the first CH bond. This study presents a density functional theory investigation of doping of cerium dioxide (111) with alkaline earth metals to promote methane activation. The incorporatation of alkaline metals in the surface results in spontaneous formation of charge compensating oxygen vacancies, and thus enhances surface reducibility. This effect from substitutional doping of the ceria surface greatly improves the adsorption, and the stablity of the $CH_3^{\cdot}$ + H dissociation products compared undoped ceria. The enhanced stabilisation of the products drives the thermodynamics towards dissociation. The calculated kinetic barriers show that for Mg and Ca doped surfaces, the kinetic barrier is lowered compared to the undoped surface, while for Sr the activation energy is higher. We find a correlation between the thermodynamics and kinetics with the cation dopant size; the dissociation products become more stable with a decrease in dopant ionic radius while the kinetic barriers are reduced with increasing cation size up to the limit of the Ca cation. A smaller dopant ionic radius compared to that of CeO_2 promotes methane activation, while doping with a larger ionic radius cation than the host diminishes the activity of the surface towards methane activation. The thermodynamics and kinetics that are affected from the dopant ionic radius show that consideration of the dopant size in a host oxide is needed for catalyst design. A simple descriptor for the reaction process is also developed arising from the relationship between the active oxygen vacancy formation and the stabilisation of the dissociation products.

Introduction

Biogas derived from the anaerobic decomposition of organic matter (biomass) is a strong potential candidate as a renewable fuel source with a small carbon footprint, and can be compressed to natural gas to be used as a motor fuel source.[1, 2] The use of biogas facilitates a sustainable energy supply and also reduces the concentration of environmental pollutants such as nitrogen and sulfur oxides, which are released from fossil fuel sources.[3] These gases can cause detrimental and irreversible damage to the environment by forming acid rain with atmospheric water which can damage crops and water ways, as well as forming smog in urban areas that affects human respiratory health.[4] There is thus a desire to develop a 'green' alternative, with biogas being one such candidate.

The utilisation of biogas as an alternative, cleaner fuel is highly desirable as it is composed primarily of methane gas (~80%), with smaller contributions from carbon dioxide, hydrogen sulfide, and siloxanes, which can be purified for applications.[5]

The activation of the biogas as a fuel or as a precursor to development of synthetic gas (syngas),[6-10] methanol,[11-15] formaldehyde,[16-20] acetic acid[21] and other biofuels[22, 23] depends greatly on the activation of the initial C-H bond by the following reaction;

$$CH_4 \rightarrow CH_3^{\cdot} + H$$

where a $CH_3^{\cdot}$ radical and H atom are formed, with a large energy cost of 440kJ/mol in the gas phase.[24] The relatively large activation energy indicates that a catalyst is required to lower the energy needed to break this bond. The subsequent successive dehydrogenation of the $CH_3^{\cdot}$ radical leading to CO/CO_2 + H_2/H_2O products, depending on the catalyst used and desired reaction process,[9, 10, 25-27] are much more facile steps than the initial C-H bond cleavage which suggests that this step is the rate limiting, and the most difficult step of the reaction process to overcome. Not only does this demanding step play significant importance in the activation of methane but also for general C-H bond activation (or C-H bond functionalisation) in hydrocarbon chemistry. There is thus a considerable interest in developing catalysts that can efficiently carry out this challenging process.

The low index (111), (110), and (100) surfaces of Ni,[28-33] Pt,[34-38] Cu,[39, 40] Pd,[41] and Rh,[42] have been investigated as potential catalysts to activate the C-H bond of methane. On all transition metal surfaces investigated for this process, exothermic dissociation of the C-H bond occurred with reported activation

---

[a] *Tyndall National Institute, University College Cork, Lee Maltings Complex, Dyke Parade, Cork City, Co. Cork, Ireland, T12 R5CP*

† john.carey@tyndall.ie, Michael.nolan@tyndall.ie

Electronic Supplementary Information (ESI) available: [details of any supplementary information available should be included here]. See DOI: 10.1039/x0xx00000x

This journal is © The Royal Society of Chemistry 20xx

energies from temperature programmed desorption of 52.7kJ/mol, 26.8kJ/mol, 55.6kJ/mol on the Ni (111), (100), and (110) surfaces, respectively.[43] Molecular beam studies have determined energies of 39-, 52-, 29- and 71 -kJ/mol on the (111) surface of Ir[44] Pt,[38] Rh,[45] and Pd[46]. Density functional theory (DFT) calculations have determined an activation energy of 105 kJ/mol on Ni(111) which is lowered by 17kJ/mol with the presence of structural defects,[47] while the Pt(111), Rh(111) and Ru(0001) surfaces have calculated barriers of 89 kJ/mol,[48] 58 kJ/mol[49] and 85 kJ/mol[50], respectively, suggesting that lower activation energies to dissociate CH_4 occur on Ir and Rh. The successive dehydrogenation on the transition metal surfaces leads to tightly bound carbon deposits causing selective poisoning of the active surface sites, rendering the catalyst surfaces inactive at higher coverages over time.[28, 51] Metal oxides such as TiO_2,[52] ZrO_2,[53] SiO_2,[54] PdO,[55] and NiO,[9] are more resistant to carbon deposits through interaction of the lattice oxygen with carbon forming CO and CO_2, and the dispersion of metal clusters is important for methane dissociation.[53] There is thus a desire to design a catalyst that is carbon (coking) resistant, and highly active for methane dissociation, while also being economical by avoiding the use of precious metals.

Cerium dioxide (CeO_2) is a strong candidate catalyst for the partial oxidation of methane. CeO_2 is a highly reducible material with many applications in heterogeneous catalysis,[56-62] solid oxide fuel cells,[63-69] ceramics,[70-73] and in the three-way catalytic converter.[74-80] The most thermodynamically stable surface is (111) which is of great interest and importance.[81, 82] The formation of neutral oxygen vacancies (Ovac) as intrinsic point defects on the surface occurs by the following process (in Kroger-Vink notation);

$$O_o^x + 2Ce_{Ce}^x \rightarrow V_o^{\cdot\cdot} + 2Ce'_{Ce} + \frac{1}{2}O_2$$

Where the O_o^x represents a neutral O on an O lattice site and Ce'_{Ce} is a negative Ce cation on a Ce lattice site. The two excess electrons reduce two Ce cations from Ce(IV) to Ce(III) from the Ovac formation, with a computed energy cost ranging from 2.00 to 2.50eV for PBE+U.[83] Facile oxygen vacancy formation in CeO_2, and the high oxygen storage capacity (OSC), play a vital role in the use of CeO_2 in many applications and in some cases it is used as a simple descriptor to predict potential candidate materials for many reactions.[84, 85] Oxidative coupling of CO to form CO_2 from lattice oxygen on the CeO_2 surface which is replenished by the dissociation of $NO_{2,}$ is an important reaction in the three-way catalytic converter for emissions control.[86-89] Reactions at the CeO_2 interface, such as the water/hydrogen cycle,[90] sulfoxide formation,[91] methanol to formaldehyde,[92] oxidative dehydrogenation of propane,[93, 94] are all greatly influenced and promoted by the OSC properties, where the surface oxygen vacancies are filled by atmospheric oxygen according to the well-known Mars Van-Krevelen mechanism.[95] The reducible properties of CeO_2 have attracted much interest for the partial oxidation of methane,[96-98] showing improvements over other metal oxides; however the computed dissociation barrier of 138 kJ/mol for the undoped CeO_2 (111) surface is particularly high compared to transition metal surfaces.[99, 100] There is thus a need to greatly improve the properties of the CeO_2 (111) surface for methane activation to facilitate oxygenation reactions on a comparable scale with transition metal surfaces.

The properties of the (111) surface of CeO_2 for both reducibility and CH_4 activation of can be greatly improved by substitutional doping of non-native transition metals at the Ce cation site.[100] The partial oxidation of methane and the C-C coupling for ethane production (C_2 selectivity) was investigated in detail on alkaline metal (Mg, Ca, Sr) doped CeO_2 by a range of spectroscopic techniques.[101] The Mg^{2+}, Ca^{2+} and Sr^{2+} cations mix into the CeO_2 lattice as substitutional ions at the Ce sites and oxygen vacancies are formed for charge compensation. Doping created highly reactive electrophilic oxygen species at the surface interface to greatly improve the oxidative coupling of methane compared to undoped CeO_2. The ionic radius of the dopant was found correlate to the reactivity for the oxidative coupling of methane and C_2 selectivity, as Mg^{2+} and Sr^{2+} which have smaller and larger ionic radius than Ce^{4+}, respectively, are found to have a decrease in activity that is attributed to the structural distortions of surface around the dopant cation. The Ca^{2+} cation does not experience this reduction in reactivity which is suggested to be due to the similar ionic radii of Ca^{2+} and Ce^{4+} cations. Substitutional doping of the low index surfaces of CeO_2 with Mg was investigated using a combination of DFT calculations and experiment showing that a +2 dopant requires a charge compensating vacancy, and also causes strong lattice distortions.[102] Enhancement of the oxygen vacancy formation and hence the OSC within the CeO_2 lattice is facilitated by doping with +2 dopants,[103] which may be useful for oxidative coupling and activation of methane. The cationic radius for a range of substitutional transition metal dopants, from group IV to XII, in the (111) surface of CeO_2 were shown to effect the adsorption energies of dissociated species, oxygen vacancy formation, and the activation of the C-H bond.[104] A volcano relationship between optimal M/CeO2 dopant for methane activation with oxygen vacancy formation, suggesting that careful consideration of the choice of dopant is necessary for the activation of methane on doped surfaces.

In this paper DFT calculations are used to investigate methane activation at the alkaline doped (111) surface of CeO_2. We first examine substitutional cation doping in the surface, and then the charge compensation of the +2 dopants. The energies for the formation of the active oxygen vacancy which is a second oxygen vacancy will also be assessed. The adsorption of CH_4 and its subsequent dissociation to CH_3^* + H is investigated in great detail, with all possible adsorption configurations considered to determine the lowest energy structure on each of the charge compensated doped surfaces. The activation energies for CH bond dissociation on each of the doped surfaces will be calculated using the climbing image nudged elastic band approach.[105-108]

The DFT calculations shows that the charge compensating oxygen vacancy is necessary to describe the correct ground state electronic structure for a charge neutral doped CeO_2 (111). The calculated energies for the active oxygen vacancy are lower than the undoped surface, indicating that doping the surface promotes oxygen vacancy formation. These energies correlate to the ionic radius of the dopant cation; the energies

Catalysis Science & Technology Accepted Manuscript

increase with increasing ionic radius, which suggests that smaller cations promote oxygen vacancy formation over larger cations. The smaller cations of Mg and Ca also improve the thermodynamics for dissociation and the kinetics for methane activation, compared to the undoped CeO_2 surface, while the larger Sr cation worsens these properties. From the calculated adsorption energies for the dissociation products and the energy to form the active oxygen vacancy, a linear relationship is observed showing a correlation between the two properties. This relationship can be utilised to provide a descriptor for further catalyst design in the activation of methane.

Computational Methodology

All calculations were performed using density functional theory within the generalized gradient approximation (GGA) using the Perdew-Burke-Ernzerhof (PBE) exchange-correlation functional,[109] as implemented in the Vienna *ab initio* Simulation Package (VASP).[110-113] The valence electrons were expanded using a plane wave basis set, with the electronic valence and core interactions being described by the projected augmented wave (PAW) method.[114] Non-spherical contributions from the gradient corrections inside the PAW radii are also included, which are important for accurate total energy calculations. To correct for the strong electronic correlation within bulk CeO_2, the DFT+*U* method,[115] [116] is used with a U parameter of 5eV[79, 80, 82, 117, 118] applied to the Ce 4*f* states for all calculations.

The Brillouin zone integrations were sampled using the Monkhorst-Pack method,[119] and *k*-point sampling grids of (2x2x2), (4x4x4) and (6x6x6) were tested on the CeO_2 bulk at a 400 and 500eV plane wave cut-off. The structural optimizations of the CeO_2 bulk were carried out using a conjugate-gradient algorithm, and performed at a series of volumes where the atomic positions, forces and cell angles were allowed to relax while keeping the cell volume constant. The resultant energies were fitted to the Murnaghan equation of state[120] to obtain the minimum energy structure. The parameters which sufficiently converged the structure to a minimum energy structure were found to be a *k*-point sampling grid of 4x4x4 at a 400eV energy cut-off with a lattice parameter of 5.408Å which deviates from the experimental structure by 0.1%.[121] The bulk, and all subsequent structures were optimised using the conjugant gradient method and deemed converged when the forces on the atoms were determined to be less than 0.02 eV/Å.

The (111) surface of CeO_2 was cut from the low energy structure of bulk CeO_2, and the slab model is periodically infinite in the *xy* direction with a vacuum gap above the surface. A slab of 12 atomic layers was used with a 15.3Å vacuum gap above the surface to remove any interactions along the *c* vector. The slab was expanded to a *p*(4x2) structure and relaxed using a similar energy cut-off to the bulk structure with a *k*-point sampling grid of (1x2x1), which is consistent with the bulk density sampling.

The reduction of the non-doped and doped (111) surface of CeO_2 is important in the activity of ceria. The surface vacancy formation energy is calculated by;

$$E_f = \left(E_{MxCe(1-x)O(2-y)} + \frac{1}{2}E_{O2}\right) - E_{MxCe(1-x)O2}$$

Where E_f is the calculated oxygen vacancy formation energy, $E_{MxCe(1-x)O2(2-y)}$ is the calculated energy of the metal doped surface with an oxygen vacancy, E_{O2} is the calculated energy of gas phase O_2, and $E_{MxCe(1-x)O2}$ is the calculated energy of the metal doped surface. As the alkaline earth metal dopants have a charge of +2, the first oxygen vacancy forms spontaneously with a negative E_f. This is referred to as the charge compensating vacancy, and the active oxygen vacancy is the next oxygen species that is removed from the metal doped surface.

The molecular and atomic adsorbates were placed on the charge compensated metal doped (111) CeO_2 surface at the top side of the slab, with the bottom CeO_2 unit (3 atomic layers) of the slab fixed to the minimum energy bulk positions. The adsorption energies were calculated by;

$$E_{(ads)} = E_{(Mol-CeO2)} - (E_g + E_{slab})$$

Where $E_{(ads)}$ is the calculated adsorption energy, $E_{(Mol\text{-}CeO2)}$ is the energy of the adsorbate on the surface, E_g is the energy of the gaseous species in a vacuum, and E_{slab} is the energy of the bare CeO_2 surface slab. A negative adsorption energy indicates a favourable interaction between the adsorbate and the surface, while a positive energy indicates a disfavoured interaction.

A symmetric slab with hydrogen adsorption on both sides of the slab was tested to examine the adsorption energy relative to the one-side adsorption. The adsorption energy changes by less than 0.1eV, which is an acceptable deviation. This is consistent with other surface science DFT studies, suggesting that there is very little difference between the symmetric adsorption and adsorption at a fixed bottom slab. The use of the fixed bottom slab overcomes complications during the calculation of climbing image nudged elastic band (CI-NEB) method. This keeps the molecule/atomic adsorption calculations, and the CI-NEB calculations consistent and comparable within this body of work. Previous studies have used the symmetric slab approach for molecular adsorptions and then changed to the fixed bottom slab for CI-NEB calculations which introduces inconsistency in the calculations, which will be avoided.

The calculated energies of the most stable adsorption modes and gas phase species are used to construct the reaction profile for the activation of methane on the bare and alkaline metal-modified CeO_2 surfaces. The CI-NEB approach, as implemented in the VASP code by Henkelman *et al.*[105-108] is used to calculate the kinetic barriers between the most stable adsorption modes along the reaction pathway. This is carried out by using the most stable adsorption modes to anchor the 'elastic band' between structures, and the transition state is

Catalysis Science & Technology Accepted Manuscript

Please do not adjust margins

pushed up to a local maximum as the turning point to provide the kinetic barrier. A vibrational calculation is used to confirm that the obtained transition state is a true maximum on the potential energy surface since it has an imaginary frequency associated with a single vibrational mode. The CI-NEB calculations are carried out using a Newton-Raphson minimisation method, and are deemed converged when the forces are less than 0.02eV/Å.

The electronic structure for the oxygen vacancy formation and each of the most stable adsorption modes will be determined by calculating the partial (ion and *l*-quantum number decomposed) electronic density of states (PEDOS) using the default atomic radii in VASP. The charges of the adsorbate and surface are calculated using Bader's atoms in molecules approach.[122-124]

Results

Undoped, reduced and alkaline doped CeO_2

The calculated structure of the (111) surface of CeO2 is shown in Figure 1(a). The Ce-O surface bond lengths are 2.35Å while the Ce-O bond lengths between layers were determined to be 2.38Å. To show the electronic structure of the undoped CeO_2 (111) surface, the PEDOS is shown in Figure 1(b). The valence band (VB) and conduction band (CB) are primarily a mixing of the Ce 4*f* states (green lines) and O 2*p* states (red lines), with no other states shown as these provide negligible contribution to the top of the VB and the bottom of the CB. The VB to Ce 4*f* gap is 2.39eV.

As CeO_2 is a well-known reducible metal oxide, it is important to characterise oxygen vacancy formation in the undoped (111) surface. From previous work on the (111) surface of ceria, it has been well established that sub-surface oxygen vacancies are preferentially formed over surface vacancies.[117] The removal of an oxygen species from the sub-surface layer reduces two Ce cations from Ce(IV) to Ce(III), with a calculated oxygen vacancy formation energy of 2.19eV. The calculated value falls within the previously reported range for oxygen vacancy formation on the CeO_2 (111) surface of 2.00 eV to 2.50 eV by PBE+U calculations.[83] A number of different Ce(III) cation positions are possible after forming the vacancy giving different energy solutions as a spread of 0.3 eV as a function of Ce(III) distributions;[83, 125, 126] Our calculated value is used as a guideline for comparing to oxygen vacancy formation in the doped surfaces.

The reduction of the Ce cations on the surface from the formation of an oxygen vacancy forms a Ce 4*f* defect peak in the band gap between the top of the valence band (VB) and the unoccupied Ce 4*f* states around 2.1eV above the VB. The defect peaks is located at 1.11eV above the VB. The defect peak is derived from the Ce 4f states which originate from the two electrons that are localised on two Ce cations. Both electrons have up spin indicating that a ferromagnetic (FM) ground state electronic structure is preferred over an anti-ferromagnetic (AFM) for the reduced CeO_2 (111) surface.[83] The reduction of the Ce cations is confirmed by Bader charges which indicate a gain of 0.32 electrons compared to the bare CeO_2 (111) surface. Spin magnetisation values of 0.99 on each reduced Ce cation further supports this mechanism.

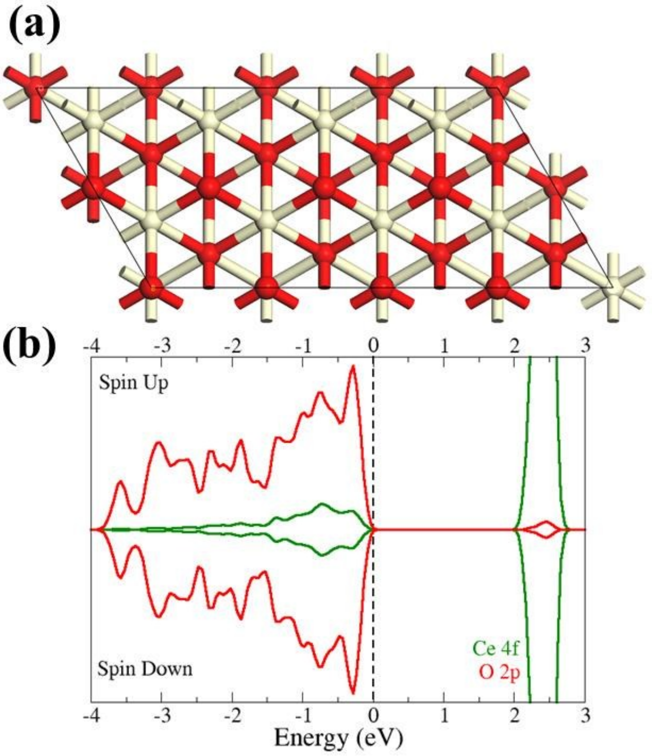

Figure 1: The calculated (a) structure, and (b) the PEDOS for the (111) surface of CeO2. The white and red spheres show the Ce cation and O anion lattice positions. The green and red lines on the PEDOS show the Ce 4f and O 2p states that contribute to the conduction and valence bands, respectively. The top of the valence band in the PEDOS is aligned to 0eV as indicated by the dotted black line.

Substitutional doping on the Ce lattice site with the alkaline metal (M = Mg, Ca, Sr) in the surface and subsurface layers was investigated. The preferential lattice position for all dopants was on the surface Ce site. Mg adopts a four coordinate distorted tetrahedral geometry, whereas Ca and Sr have square pyramidal and octahedral coordination in the lattice. These alkaline earth metal dopants increase in ionic radius down group II from Mg (0.57Å) to Ca (1.00Å) to Sr (1.18Å), which facilitates the increase in coordination number of the dopants on the surface. The substitutional doping of the Ce cation by the alkaline metal dopants, which have an effective charge of +2, removes two electrons from the system, creating effective charges of +1 on two neighbouring oxygen atoms relative to lattice oxygen becoming O^-, which are normally referred to as hole states. In order to balance the creation of two +1 charges in the system, a charge compensating oxygen vacancy must be introduced into the system. The lattice position of the most stable charge compensating oxygen

Catalysis Science & Technology Accepted Manuscript

vacancy to the dopant cation was investigated by examining the energetics of removing different oxygen atoms. The possible choices for the oxygen vacancy are the nearest neighbour (nn) and next nearest neighbour (nnn) oxygen atoms in the surface (surf) and sub-surface (sub) in the sub layers as shown in Figure 2.

Examining the oxygen vacancy formation energies for the removal of the different oxygen atoms, the preferential position of the charge compensating vacancy for Mg was found to be the nn-surf, while Ca and Sr preferred the nn-sub and the nnn-sub surface positions, respectively, as shown by the black spheres in Figure 3. The smaller Mg cation appears to promote surface vacancies, while the larger Ca and Sr cations favour sub surface oxygen vacancies similar to the undoped surface. The calculated formation energies for the charge compensating vacancies are -1.26eV, -1.01eV, and -0.85eV for Mg, Ca and Sr dopants. The values decrease with increasing cation radius suggesting that there is a correlation between the dopant size and vacancy formation energies. The negative formation energies indicate spontaneous formation of oxygen vacancies, associated with charge compensating species.

The electronic structure was examined for the most stable charge compensating vacancy in each of the doped surfaces. The calculated PEDOS for each of these systems was found to have similar characteristics, as shown for the example of Mg-doped CeO_2 in Figure 4, with no substantial contribution from the dopant to the top of the VB and the bottom of the CB. For each of the dopants, the M 2*p* states are at the bottom of the VB (around -40eV) and are not shown on the graph. The calculated PEDOS has similar characteristics to the undoped (111) surface of CeO_2 (Figure 1) with no defect peaks in the band gap, and shows that the holes on the oxygen atoms from the initial doping of the alkaline metal in the surface have been quenched by the release of the two electrons from the oxygen vacancy. The ground state structures of the doped surfaces are therefore charge neutral. This was also confirmed by Bader analysis as the charges on each of the atoms in the doped surface with oxygen vacancy and undoped surface are similar, while examination of the spin states show no excess spins. The charge compensating vacancy is mandatory to properly describe the ground state electronic structure of the system. This is necessary for further investigation of surface reactions as an incorrect description may produce inaccurate and often spurious results due to over-binding of molecular and atomic adsorbates.

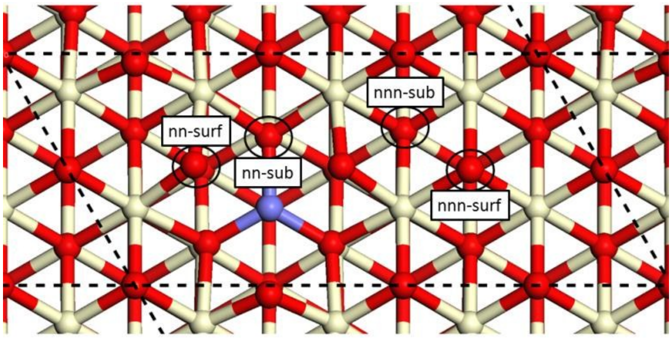

Figure 2: The lattice positions of the oxygen vacancies relative to the dopant. The white, red and purple spheres are the lattice positions of the Ce, O and M atoms.

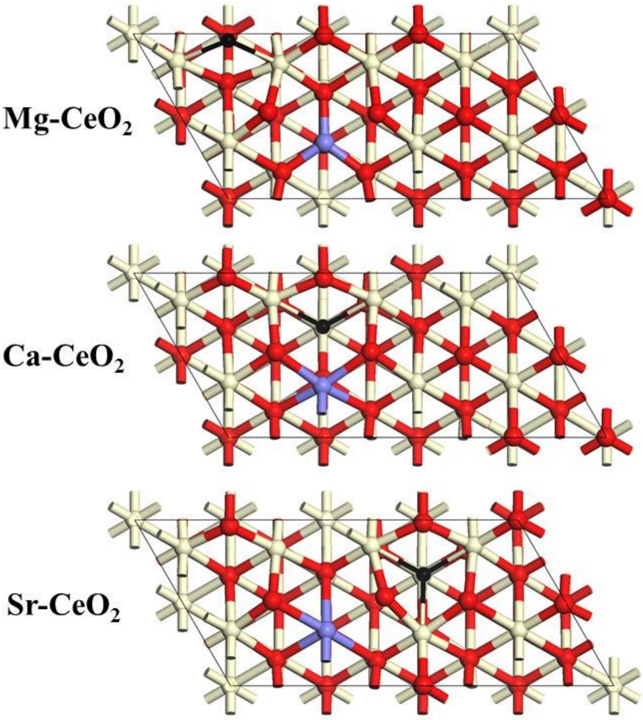

Figure 3: The calculated structures for the most stable configuration of the charge compensating oxygen vacancy, on the Mg, Ca, and Sr doped (111) surfaces of CeO_2. The white, red, and purple spheres are the lattice positions for the Ce cations, O anions, M dopant with the location of the oxygen vacancy indicated by the black sphere.

The removal of a second oxygen atom from the already charge compensated surface structure forms a second vacancy, which is referred to as the ‘active oxygen vacancy’. The lowest energy configuration for the active oxygen vacancy of each doped surface was explored by starting from the charge compensated

Catalysis Science & Technology Accepted Manuscript

Please do not adjust margins

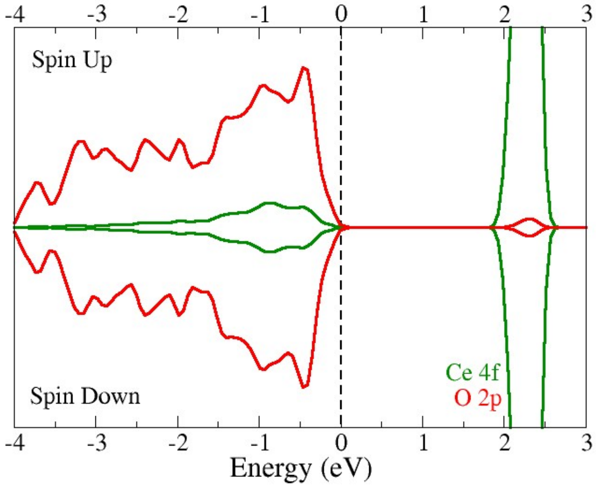

Figure 4: The calculated PEDOS for the Mg-doped (111) surface of CeO_2 with the charge compensating vacancy. The green and red lines are the Ce 4*f* and O 2*p* states. The top of the VB is aligned to 0eV

structure (Figure 3), and removing other possible oxygen atoms in the surface, as shown in Figure 2.

Considering all other nearest neighbour and next nearest neighbour combinations with the charge compensated structure, the lowest energy structure for the active oxygen vacancy in the Mg, Ca and Sr doped (111) surface of CeO_2 are shown in Figure 5(a), (b) and (c), respectively. For Mg-doped CeO_2 (111), the calculated active oxygen vacancy is the nnn-sub surface oxygen to the left of the dopant site. The removal of this oxygen species results in migration of a surface oxygen atom, which is indicated by the orange atom on the figure. The relaxation of the surface oxygen atom into the sub-surface vacancy leaves a nn-surface oxygen vacancy, indicated by the blue sphere on the figure. This leaves two neighbouring surface oxygen vacancies, the charge compensated (black sphere) and active vacancy (blue sphere), giving an unusual next nearest five coordinated Ce cation to the Mg dopant. The preferential formation of vacancies in the surface layer is strongly promoted by the presence of the Mg dopant, and causes a highly distorted surface structure. This may leave under-coordinated active surface species and/or sites that would play an important role for surface catalytic reactions.

The removal of the oxygen atom and creation of the active surface vacancy reduces the two nearest neighbour Ce cations from Ce(III) to Ce(IV), which is illustrated by the calculated spin density iso-surface shown in Figure 5(a). The figure shows the highest spin arrangement to indicate the location of the reduced Ce cations, as there is a small difference of 0.01eV between the AFM and FM arrangements. We show the most stable active oxygen vacancy site in each case. Supporting information shows formation energies of the other trialled vacancy sites. The reduction of the Ce cations is also evident in the calculated PEDOS, with the appearance of a defect peak in the band gap around 1.00eV from the top of the VB. Bader charge analysis confirms that the two Ce cations are reduced with a gain of 0.3 electrons. The in-gap PEDOS is associated with one electron localised on the 7-coordinated Ce(III) cation that is furthest away from the Mg dopant. Further investigations into the band occupations reveals that a defect peak associated with the unusual 5-coordinate Ce(III) cation is greatly lowered in energy to such an extent that it is located within the top of the VB, and not observable on the plot. This defect peak being located in the VB may have occurred by the change in coordination of the Ce(III) cation due to the two neighbouring oxygen vacancies, thus greatly stabilising the cation and lowering the Ce 4f^1 electron in energy below the top of the VB.

The calculated lowest energy configuration for the active oxygen vacancy for Ca and Sr -doped CeO_2 (111) is not as complicated as Mg since these atoms have large cation radius and can adopt a similar coordination environment to the Ce cations. For both dopants, the preferential oxygen vacancy is an oxygen atom bonded to the dopant, forming next nearest neighbour sub-surface vacancies as shown by the blue spheres in Figures 5(b) and (c). The calculated spin density for each dopant structure shows that the removal of the oxygen atom reduces two Ce cations from Ce(IV) to Ce(III). For Ca-doped CeO_2 (111), the two reduced Ce cations are nearest neighbours to the oxygen vacancy with one in the surface and the other below the vacancy in the sub surface layer. Relative to the Ca cation, however, the reduced Ce cation in the sub surface is nearest neighbour, and the reduced Ce cation in the surface is next nearest neighbour. As these reduced Ce(III) cations are in different coordination environments, two separate defect peaks appear in the band gaps as shown in the calculated PEDOS. The larger cation radius of Sr dopant in CeO_2 causes the reduced Ce(III) cations to be located next-nearest neighbour and next-next nearest neighbour to the dopant as shown by the spin density plots in Figure 5(c). Similarly to Ca-doped CeO_2, two defect peaks appear in the band gap of the calculated PEDOS plot for Sr-doped CeO_2 which are associated with the two reduced Ce(III) cations.

The calculated formation energies for the active oxygen vacancy in Mg, Ca, and Sr doped CeO_2 (111) are +1.22eV, +1.78eV, and +1.90eV. The positive value of the formation energies show that energy is required to remove the oxygen atom, which is normally the case with oxygen vacancies in metal oxides. This shows the importance of charge compensation, and determining the correct ground state electronic structure. The calculated energies are seen to correlate with increasing ionic radius of the dopant cation indicating that oxygen removal and vacancy formation are more difficult for larger cations. The lower vacancy formation energy of Mg may be attributed to the small ionic radius causing strong distortions in the lattice.

Catalysis Science & Technology Accepted Manuscript

This journal is © The Royal Society of Chemistry 20xx

Please do not adjust margins

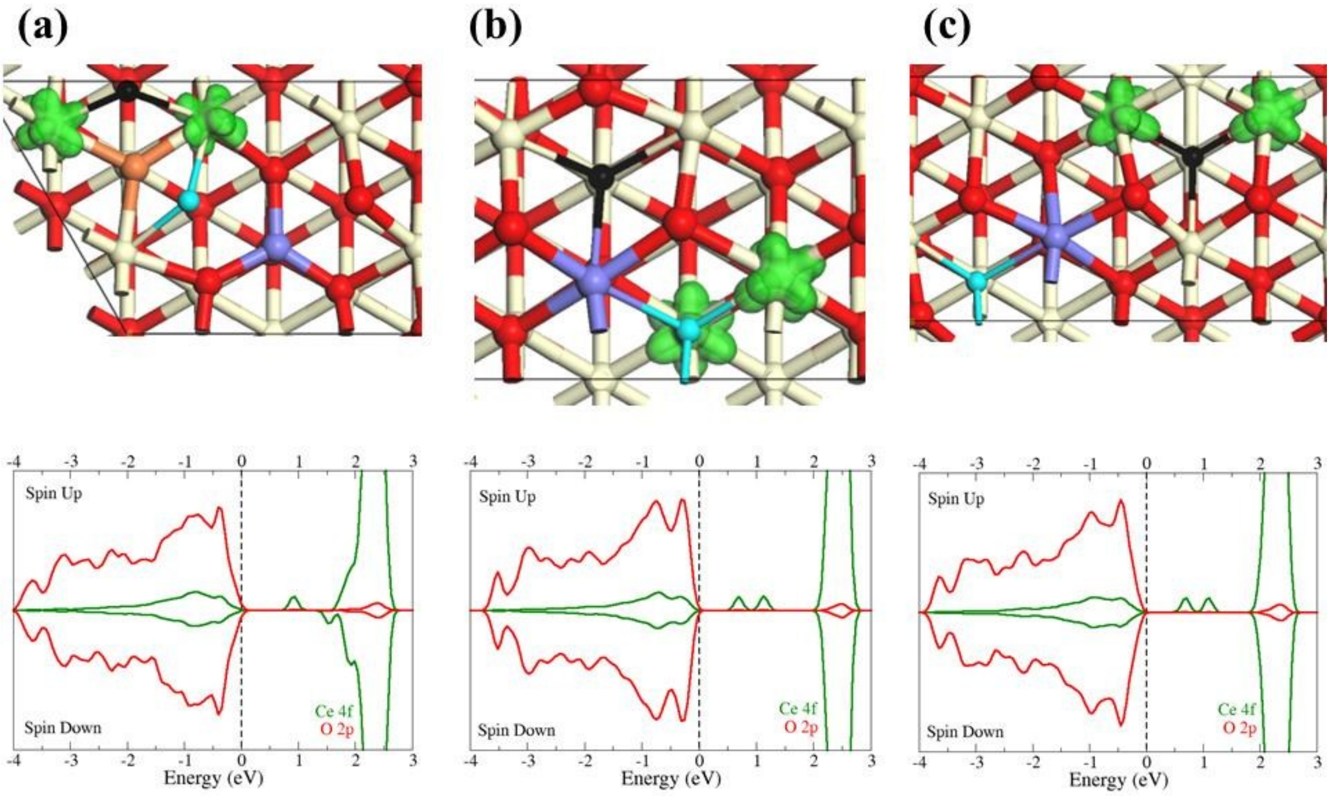

Figure 5: The calculated lowest energy configuration for the active oxygen vacancy of (a) Mg, (b) Ca and (c) Sr doped CeO_2 (111), along with the associated PEDOS plots. Only the local structure around the dopant is shown for clarity. The white, red, and purple spheres are thelattice positions for the Ce, O, and M dopant atoms. The charge compensated oxygen vacancy is indicated with the black sphere on the surface, while the active vacancy is indicated with a blue sphere. The green iso surface (0.05 electrons $Å^{-1}$) indicates the position of thereduced Ce(III) cations on the surface. The green and red lines on the PEDOS plots are the Ce 4*f* and O 2*p* states, and the plots are aligned to the top of the VB.

Molecular and atomic adsorption on alkaline metal doped and bare (111) surface of CeO_2

To assess the catalytic properties of alkaline earth metal doped CeO_2 for methane activation, the adsorption process and electronic structure of CH_4, CH_3 and H on each of the doped surfaces, and undoped CeO_2 (111) have been investigated. To achieve this, the lowest energy configurations on each of the doped/undoped surfaces are determined from exploring all possible adsorption modes at different adsorption sites. The possible adsorption sites on the charge compensated structure are shown in Figure 6, for the example of the Sr doped CeO_2 surface. There are four different kinds of adsorption sites; (I) the nearest 3 fold O atom to the dopant, (II) the exposed dopant cation, (III) the 2 fold oxygen species laying between the dopant and vacancy, and (IV) the 3 fold oxygen atom close to the vacancy. Similar adsorption sites are possible on both the Mg and Ca doped surfaces. The bare (111) surface of CeO_2 is not as complicated as the doped surfaces since all surface oxygen atoms are equivalent by symmetry for CH_4, CH_3 and H adsorption.

The orientation, interaction and adsorption of molecular CH_4 was investigated on the bare (111) surface of CeO_2. The CH_4 molecule is found to weakly interact (E_{ads} = 0.1eV) with the surface in a physisorbed state 3Å above the surface, as shown in Figure 7(a). The preferred orientation has two H atoms pointed towards the surface, which is 0.1eV more stable than other possible orientations such as a single H atom pointed to the surface[104] or flat with 3 H atoms close to the surface.[99, 100]

The difference in energies is not significant at 0K, however considering 0.1*k*T at 298K this value becomes more significant suggesting that vibrational and rotational contributions to the partition function for the activation of methane play an important role as observed for Ni surfaces.[29] Van der Waals corrections are not employed for the physisorbed CH_4 molecule as these corrections only add around 0.01eV to the total energy which is a negligible contribution to this adsorbate as it is essentially still in the gas phase.

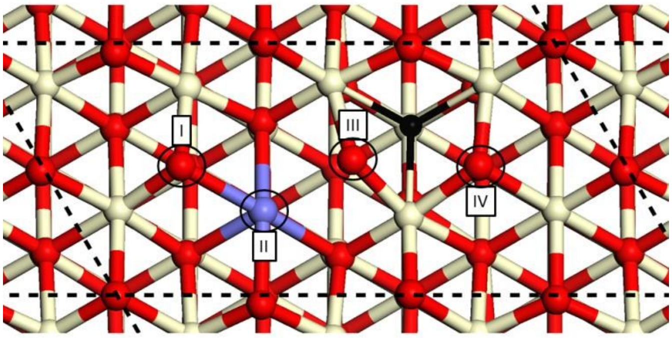

Figure 6: The charge compensated structure of Sr doped CeO2 (111). The different adsorption sites to examine for molecular and atomic adsorption are numbered I-IV.

Catalysis Science & Technology Accepted Manuscript

Please do not adjust margins

Catalysis Science & Technology Accepted Manuscript

The calculated structure for the adsorption of the dissociated products, CH$_3^{\cdot}$ and H, is shown in Figure 7(b), with both adsorbates adsorbing on surface oxygen atoms. These are the only available surface sites for adsorption due to the surface symmetry. The adsorbates form methoxide (O-CH$_3$) and hydroxyl (OH) species on the surface with calculated adsorption energy of -1.11eV, relative to gaseous CH$_4$. The surface Ce-O bond lengths increase from 2.35Å to a range of 2.58-2.60Å around the adsorbate species on the surface which indicates that the surface is distorted upon interaction with the adsorbates. The O-C, C-H and O-H bond lengths were calculated to be 1.43Å, 1.10Å and 0.97Å, respectively, showing that the C-H bond are slightly lengthened by 0.02Å compared to gaseous CH$_4$, while the OH bond is typical of surface hydroxyls.

As the radical CH$_3^{\cdot}$ and hydroxyl species are known electron donors, they are expected to transfer electron density to the surface. The calculated spin density for the interaction of the adsorbates with the surface shows that each adsorbate transfers an electron to the surface, reducing two surface Ce cations, as shown by the green isosurface in Figure 7(b). The figure shows the highest spin arrangement to indicate the location of the reduced Ce cations. The electron donation is supported by calculated Bader analysis, which shows that the adsorbed H atom becomes neutral on adsorption, while the nearest Ce cation gains 0.3*e*. For the CH$_3^{\cdot}$ species, the adsorbed C atom loses 0.8*e* and the nearest Ce cation gains 0.3*e*.

The calculated PEDOS for the adsorption of CH$_4$ and the dissociation products are shown in Figures 8(a) and (b). The VB and CB are dominated by the surface O 2*p* and Ce 4*f* states, with the molecular C 2*p* states and H 1*s* states magnified (x25) to show their contributions to the electronic structure. The H 1*s* and C 2*p* contributions to the molecular orbitals (MO) are stabilised in energy from -3.2eV in the PEDOS of the CH$_4$ molecule (Figure 8(a)) to -5.3eV in the PEDOS of the CH$_3$ + H species (Figure 8(b)) from the interaction with the CeO$_2$ surface. The appearance of an H 1*s* peak at the top of the VB for the CH$_3^{\cdot}$ radical can be associated with the creation of a σ-SOMO from the H abstraction which is a well-known characteristic for the MO description of a methyl group.[127] The presence of a defect level in the band gap around 1eV appears from the reduction of the Ce(III) surface cations, in line with the calculated spin density (Figure 7(b)). Integration of this peak reveals that two electrons are present from the two Ce(III) cations, one peak is present due to the symmetry of the reduced cations.

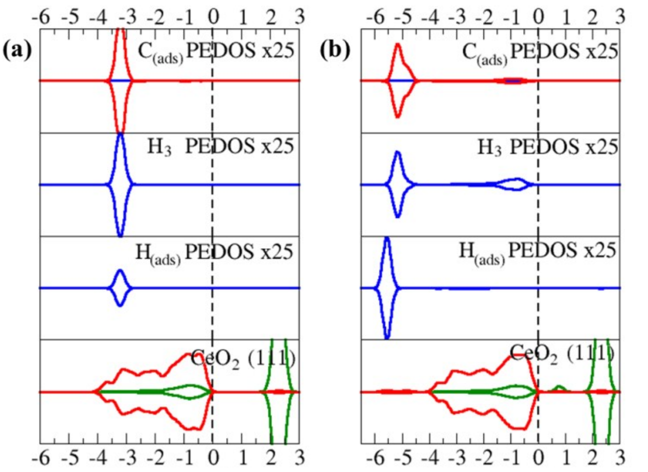

Figure 8: The calculated PEDOS for (a) CH$_4$ and (b) CH$_3$ + H adsorption on the (111) surface of CeO$_2$. The blue, red, and green lines are the *s*, *p* and *f* state contributions to the VB and CB. The top of the VB is aligned to 0eV as indicated by the dotted line.

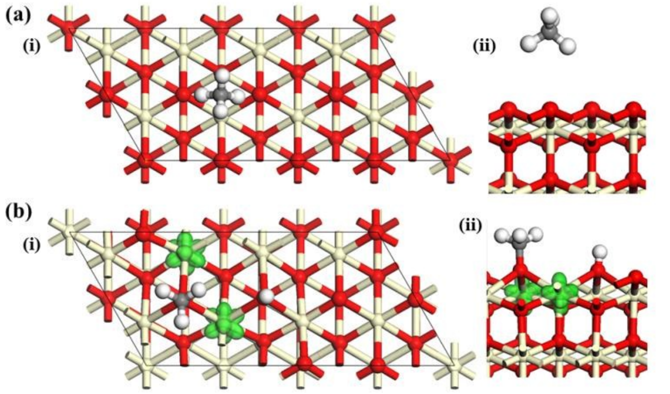

Figure 7: The adsorption of (a) CH4 and (b) CH3 + H on the (111) surface of CeO2 along the (i) *c* and (ii) *b* vectors. The green isosurface (0.05 electrons Å-3) shows the lattice positions of the reduced Ce surface cations. The off-white, red, grey and white spheres are the lattice positions of the Ce, O, C and H atoms.

Investigating the adsorption and interaction of CH$_4$, CH$_3^{\cdot}$ and H on the doped surface is more complicated due to the breaking of the surface symmetry by the dopants. The examination of the adsorption and interaction of the CH$_4$ molecule on the Mg, Ca and Sr doped surfaces indicates that the molecule weakly physisorbs around 3Å above the surface with no gain in energy, indicating there is a negligible interaction with the doped surfaces as seen for the undoped (111) surface (Figure 7(a)). The calculated PEDOS plots, Bader analysis and spin density also confirmed that the electronic structure of the CH$_4$ molecule does not change above a doped surface, in a similar manner to the bare surface (Figure 8(a)).

All possible configurations were explored for H adsorption on each of the doped surfaces as a starting point, with the lowest energy structures for the Mg, Ca and Sr doped (111) surfaces of CeO$_2$ shown in Figure 9(a), (b) and (c) respectively. The adsorption of hydrogen atoms forms surface hydroxyls with a calculated O-H bond length of 0.97Å. One electron is donated to the surface, reducing a neighbouring Ce surface cation from Ce(IV) to Ce(III) as shown by the isosurface plots in Figure 9. Bader charge analysis confirms that electron density is donated from the H atom to reduce the Ce surface cation. The O-Ce bond length increases from 2.38Å to 2.54Å, which is typical of Ce(III) formation.

This journal is © The Royal Society of Chemistry 20xx

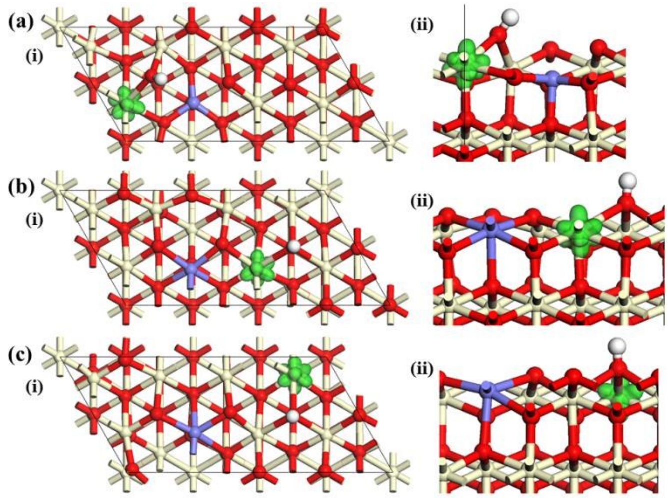

Figure 9: The The adsorption of structure of H adsorption on the (a) Mg, (b) Ca, and (c) Sr -doped (111) surface of CeO_2, along the (i) *c* and (ii) *b* vectors, where the local structure is shown for (ii). The green isosurface (0.05 electrons Å^{-3}) shows the location of the reduced Ce cation on each surface. The off-white, red, purple, and white spheres are the lattice positions of the Ce, O, dopant and hydrogen atoms, respectively

The location of the adsorbed H atom on the surface is dopant dependant; the preferred adsorption site for Mg-CeO_2 is an oxygen atom next to the dopant cation, while for Ca-CeO_2 and Sr-CeO_2 the H atom adsorbs at the next nearest neighbour O atom. The reduced Ce(III) cation is further away from the dopant site with increasing dopant ionic radius. This is caused by the Ce(III) cation having a larger ionic radius than Ce(IV), and the surface cannot accommodate two large cations, Ce(III) and Sr, being next neighbour to each other. The calculated adsorption energy for the most stable adsorption site on the Mg, Ca and Sr doped (111) surface of CeO_2 are -1.72eV, -1.47eV and -1.34eV, relative to gaseous H_2, which is more stable for Mg and Ca doped CeO_2 than H adsorption on the undoped CeO_2 surface (-1.45eV). The adsorption energies suggest that adsorption of the hydrogen atom weakens with increasing ionic radius of the dopant species.

The PEDOS for hydroxyl formation on each of the doped surfaces are found to have similar characteristics with the CB and VB being dominated by Ce 4*f* and O 2*p* surface states (Figure 10). The contribution from the adsorbed H atom and the dopant cation to the VB and CB is negligible. There is a defect peak in the band gap which is associated with the reduction of Ce cations in the surface, as shown by the isosurface in Figure 9.

The most stable adsorption modes established for H adsorption on each of the doped surfaces were used as a starting point for the co-adsorption of the $CH_3^{\cdot}$ radical species. The adsorption of the $CH_3^{\cdot}$ radical was explored on all possible adsorption sites (Figure 6) relative to the most stable H adsorption structure. The lowest energy configurations for the adsorption of $CH_3^{\cdot}$ + H on the Mg, Ca, and Sr doped (111) surfaces of CeO_2 are shown in Figure 11 (a), (b) and (c). For all surfaces, the $CH_3^{\cdot}$ radical prefers to adsorb on the nearest neighbour surface oxygen species to the dopant cation, forming a methoxide surface species (O-CH_3). The adsorbed $CH_3^{\cdot}$ on the Mg and Ca doped surfaces tilts away from the surface normal towards the dopant cation, while on the Sr doped surface $CH_3^{\cdot}$ lies perpendicular to the surface, similar to undoped CeO_2. The O-C and H-C bond lengths for the radical species are the same on all doped surfaces. The O-C bond is 1.42Å, the H-C bond is 1.11Å, and O-Ce surface bonds lengthen to 2.56Å. Both the $CH_3^{\cdot}$ and H species adsorbing near the Mg dopant suggests that the reaction centre is localised for Mg-CeO_2, while for the Ca and Sr, the dissociation takes place away from the dopant cation, which may be an effect of the large ionic radius associated with Ca and Sr, and accommodating large Ce(III) cations.

The adsorption of the radical species on the doped surfaces reduces a surface Ce cation in a similar way to the adsorption of hydrogen, as shown by the spin density plots in Figure 11. The presence of two electron donating species reduces two Ce cations, and the figures show the highest spin arrangement to indicate the location of the reduced Ce cations. The positions of the Ce(III) cations were obtained from full geometric relaxation, and different positions of the Ce(III) cations in each of these structures were not explored due to the very large number of possible configurations to examine. The difference in energy of the different Ce(III) locations in the surface would be ca. 0.1 eV, which is very small compared to the computed adsorption energies, and would not change the overall trends. Bader charge analysis confirms the reduction of the surface with two reduced Ce cations shown in Figure 11. The calculated adsorption energies for the co-adsorption of $CH_3^{\cdot}$ + H are -1.83eV, -1.40eV, and -1.29eV relative to gaseous CH_4, for the Mg, Ca, and Sr doped (111) surfaces of CeO_2 respectively, showing that Mg has the strongest interaction and Sr has the weakest interaction with the dissociation

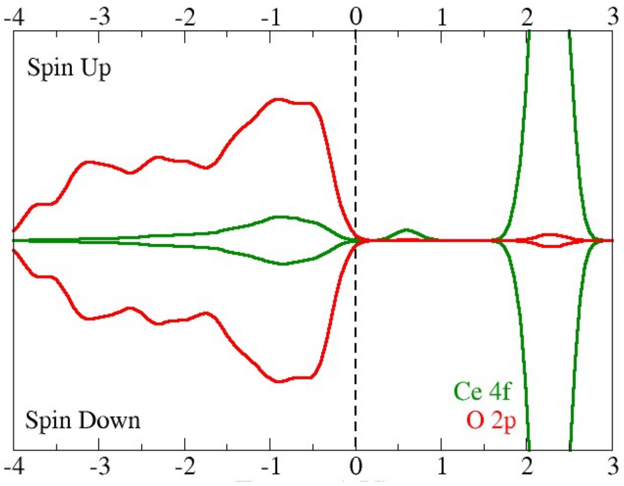

Figure 10: The calculated PEDOS for H adsorption on Mg doped CeO_2 (111). The green and red lines are the Ce 4*f* and O 2*p* states. The top of the VB is aligned to 0eV, as indicated by the dotted line green and red lines are the Ce 4*f* and O 2*p* states. The top of the VB is aligned to 0eV, as indicated by the dotted line

Catalysis Science & Technology Accepted Manuscript

Please do not adjust margins

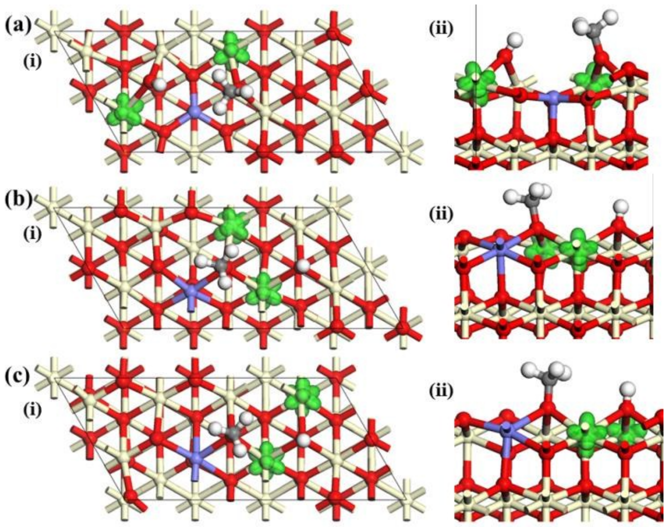

Figure 11: The most stable configuration for the co-adsorption of $CH_3^{\cdot}$ + H on the (a) Mg, (b) Ca, and (c) Sr doped (111) surfaces of CeO_2, along the (i) *c* and (ii) *b* vectors. The green isosurface (0.05 electrons Å^{-3}) indicates the lattice position of the reduced Ce cations. The off-white, red, purple, grey and white spheres are the lattice positions of the Ce, O, dopant, C and H atoms

species, but still more stable than the undoped CeO_2 (111) surface (-1.11eV). The co-adsorption energies are more stable than single adsorption on the doped surfaces, indicating an extra stabilisation of the methoxide species. This can be attributed to the acid-base interaction on doped oxides, as the hydrogen species acts as an acid on the surface which increases the binding energy of the base species (methoxide).[128, 129] The calculated energies follow a similar trend to surface hydroxyl formation, decreasing with increased atomic radius of the dopant cation. Dissociation of CH_4 is more favoured on all doped surfaces, and hence doping promotes the thermodynamic drive to form the reaction products.

The calculated PEDOS plots for the most stable configuration of the co-adsorption of $CH_3^{\cdot}$ + H on the Mg, Ca and Sr doped CeO_2 (111) surfaces are shown in Figure 12. The PEDOS shows a mixing of the C 2*p* states and H 1*s* states to the σ MO around -5 eV in the $CH_3^{\cdot}$ radical on each doped surface, and proceeding from Mg to Sr a splitting of the C 2*p* states occurs arising from stabilisation of the adsorbate on the CeO_2 (111) surface. This stabilisation occurs from the interaction with the Ca/Sr *p* and *d* states as shown in the PEDOS plot, while for Mg-CeO_2 there is no interaction between the Mg states and $CH_3^{\cdot}$ states. The σ-SOMO of the $CH_3^{\cdot}$ radical is located at the top of the VB and is broadened from the strong interaction of this orbital with the CeO_2 surface states. For Mg-CeO_2, the position of this orbital is higher in energy and closer to the top of the VB than on the other doped surfaces, suggesting donation from this orbital to the CB of the CeO_2 surface is easier since the energy gap is smaller. This may account for the greater stabilisation of $CH_3^{\cdot}$ on Mg-CeO_2, and the decrease in energy of this orbital follows the same trend as the calculated adsorption energies.

The PEDOS shows the electronic structure for the H atoms in different environments; H atoms bonded to the C atom called H_3, and the surface adsorbed H species called H_{ads} (Figure 12). For the H species adsorbed on the surface, the plot shows that some mixing occurs between the H 1*s* states and the O 2*p* states of all doped CeO_2 (111) surfaces, with the H 1*s* states lowering in energy from Mg to Sr. These states are slightly lower in energy than the H atoms of the $CH_3^{\cdot}$ states due to the direct interaction and stabilisation with the CeO_2 surface.

The position of the defect level in the band gap around 1eV is associated with the reduction of the two Ce surface cations from the adsorption of the radical and hydroxyl species. This peak is split for Mg-CeO_2 and Sr-CeO_2, while for Ca-CeO_2 it is a

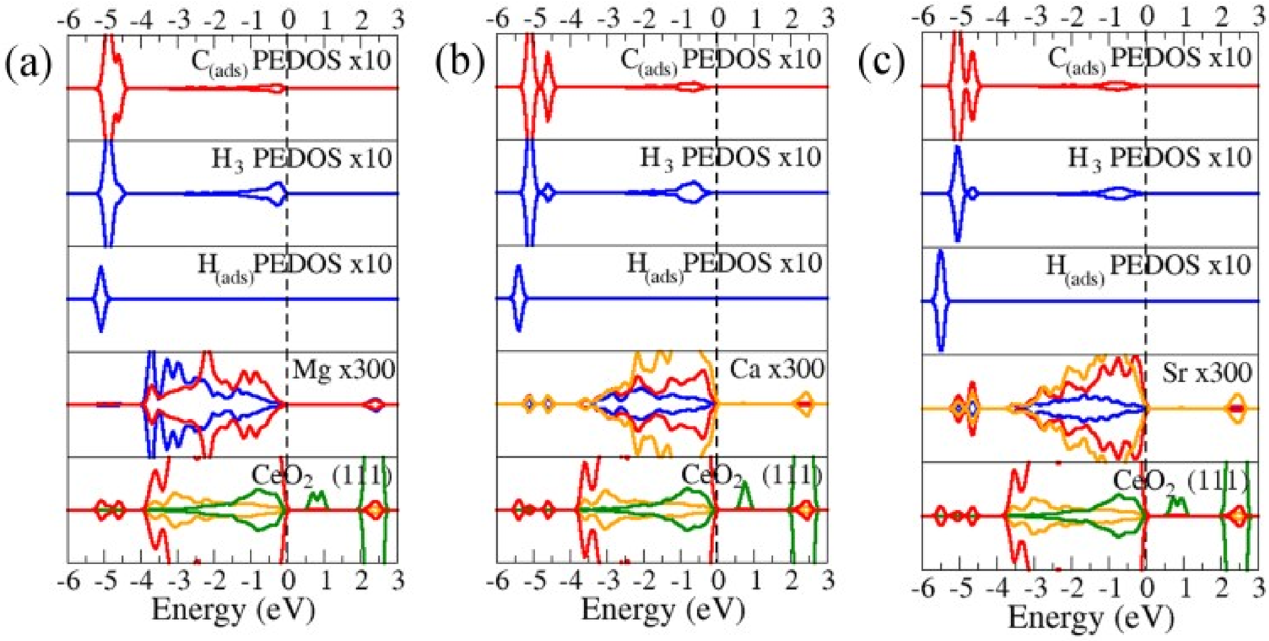

Figure 12: The calculated PEDOS plot for most stable CH_3 + H adsorption configuration on the (a) Mg, (b) Ca, and (c) Sr doped (111) surface of CeO_2. The blue, red, orange and green lines are the *s, p, d,* and *f* state contributions to the VB and CB of each system. The top of the VB is aligned to 0eV as indicated by the dotted line.

Catalysis Science & Technology Accepted Manuscript

single peak arising from the symmetry associated with the lattice positions of the two Ce(III) cations in the latter case.

The kinetic barriers for the dissociation of CH_4 to $CH_3^{\cdot}$ + H on the bare and alkaline metal doped (111) surfaces of CeO_2

The kinetic barriers were determined by using the lowest energy structures for the CH_4 and $CH_3^{\cdot}$ + H adsorption outlined in the previous sections to anchor the starting (CH_4) and end points ($CH_3^{\cdot}$ + H) of the CI-NEB calculations. The calculated structures for the transition state, on the bare and doped (111) surfaces of CeO_2 are shown in Figure 13. The calculated structure for the transition state shows that for all doped surfaces, the reaction pathway initially proceeds by H abstraction from the CH_4 molecule to form the surface hydroxyl species with the CH_3 radical unbound above the surface. The $CH_3^{\cdot}$ radical species adopts a planar geometry and is tilted relative to the surface for Mg and Sr doped CeO_2. The change in geometry of $CH_3^{\cdot}$ facilitates the formation of the surface O-C bond to form the methoxide surface species. The structure of the CH_3 species for the transition state on Ca doped CeO_2 is different with a pyramidal geometry, allowing the interaction of cerium and carbon with a Ce-C bond distance of 2.54Å. For the final structure of the dissociated species, the O-C bond forms and the three H atoms of the CH_3 species change from the planar position of the transition state (Mg and Sr), to a tetrahedral geometry with the H atoms pointed away from the surface. The calculated overall spin magnetisation of the transition state structures for the undoped, Mg and Sr doped CeO_2 (111) surface were determined to be 1. The spin magnetisation and Bader values indicate that the adsorbed H atom reduces a Ce cation, while the methyl radical is in the gas phase. For Ca-doped CeO_2 (111), the overall spin of the transition state is 2 from the reduction of two surface Ce cations by the adsorbed CH_3 and H species.

The calculated activation energies for the CeO_2, Mg, Ca, and Sr doped CeO_2 are 1.45eV, 1.32eV, 1.15eV and 1.60eV, respectively. The activation energy for the bare CeO_2 (111) surface is similar to previous DFT studies.[99, 100] For the Mg and Ca doped (111) surfaces of CeO_2, the activation energies are smaller than on the undoped surface indicating that doping the surface enhances methane activation of CeO_2, while the Sr doped surface has a larger activation energy suggesting it is worse for methane activation. The calculated lower barriers of Mg and Ca doped suggest that the reaction will proceed at lower reaction temperatures than on undoped CeO_2.

The Ca doped surface has the lowest activation energy which is attributed to the stabilisation of the transition state through the new Ce-C bond and formation of the pyramidal geometry in the transition state. The Ca dopant promotes formation of an oxygen vacancy that is a next nearest neighbour in the sub-surface layer, and a surface oxygen species becomes two fold coordinate to compensate for the absence of the oxygen atom. The formation of the two fold surface oxygen removes a Ce-O bond from a surface Ce cation, so that this Ce cation is under-coordinated which allows the Ce-C bond to form in the transition state which is not observed for the transition states on the other doped surfaces. The lower activation barrier from the stabilisation of the transition state suggests an explanation as to the experimentally observed increase in methane activation on Ca doped over the other alkaline metal doped surfaces.[101]

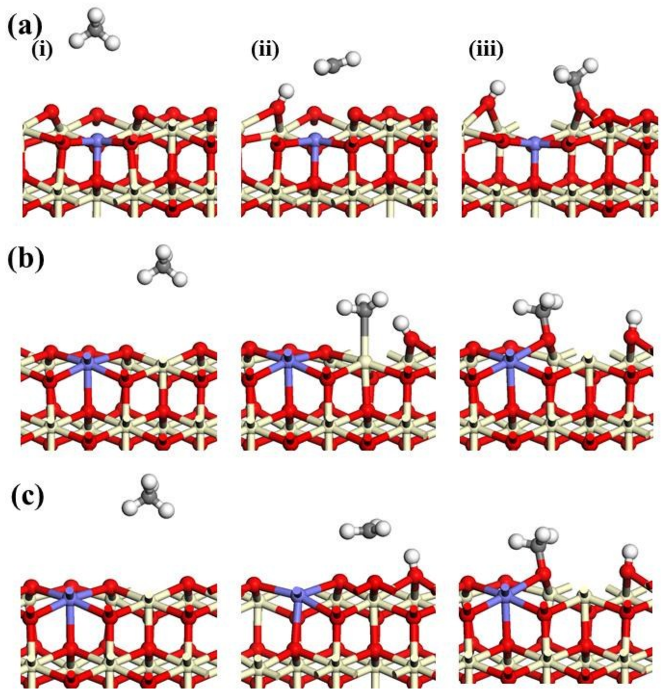

Figure 13: The calculated structures of the (i) CH_4 molecule, (ii) transition state, and (iii) dissociation products for (a) Mg, (b) Ca, and (c) Sr doped (111) surface of CeO_2.

The observation of the stabilised transition state for Ca doped CeO_2 is only possible by obtaining the correct ground state structure by taking into account a charge compensating oxygen vacancy, since its location relative to the dopant plays a vital role in describing the correct transition state structure. These results show the importance of having the correct ground state electronic structure by the inclusion of a charge compensating vacancy to correctly model reaction mechanisms on doped surfaces where charge balance is needed.

Discussion

The results presented in this paper for oxygen vacancy formation, adsorption energies of the dissociation products and activation energies for bare and doped CeO_2 (111) all show an ionic radius effect arising from the dopant cation. For all these quantities, there is a promotion effect from the presence of the dopant over the bare CeO_2 (111) surface indicating that doping the surface with alkaline metals improves the reducibility of the surface and methane activation.

Catalysis Science & Technology Accepted Manuscript

Please do not adjust margins

Both the formation of the active oxygen vacancy and the adsorption energies of $CH_3^{\cdot}$ + H become less favourable which correlates with increasing dopant ionic radius, but still shows a promoting effect over the undoped surface. The Mg cation promotes oxygen vacancy formation to a greater extent than both Ca and Sr, arising from the larger distortions present at the surface since it is a smaller dopant. Mg shows greater thermodynamic selectivity for the dissociation products, which becomes less favourable down the group II alkaline metals. For the activation energies, the Mg and Ca dopants promote the activation of methane over the undoped CeO_2 (111) surface, having lower energies than the undoped surface, and methane will be decomposed at lower temperatures. This shows that the activation of methane is improved to the limit of Ca doping, and there is no improvement in methane activation with Sr doping since this activation energy is higher than the undoped CeO_2 (111) surface. The promotion of methane on Mg and Ca doped surfaces correlates with the dopant cation radius being smaller than the Ce cations, while Sr doping which has a larger ionic radius than the host cation and appears to inhibit further promoting effects for methane activation.

The calculated energies, and correlation between the surface properties and dopant ionic radius size in this work on divalent alkaline earth metals in CeO_2 cannot be compared to previous studies on divalent transition metal dopants in CeO_2 (111),[100, 104] as a charge compensating vacancy approach is used in this work, and neglected in other reports. The inclusion of a charge compensating vacancy is vital to correctly describe the ground state electronic structure of divalent dopants in CeO_2. The omission of a charge compensating vacancy can lead to negative oxygen vacancy energies, over-binding of surface adsorbates and incorrect descriptions of transition states.[100, 104] For this reason, the energies for the properties in this work do not adhere to similar trends on transitions metal doping of CeO_2;[104] however considering the correct energies for adsorption and active oxygen vacancy formation in Mg, Ca and Sr doped CeO_2, these dopants show an improvement in methane activation on CeO_2 compared to higher valence dopants such as W, and V doped CeO_2 (111).[104]

The correlation observed in this study between the thermodynamics and kinetics for methane activation, and the increasing size of the alkaline earth meal dopant cation down group II is restricted to doping of CeO_2. Examining doping of CeO_2 with different sized cations could potentially support the role of the dopant ionic size on the behaviour of the oxide catalyst. Further work on these concepts would extend the concept beyond this work to predict, and rationally design catalysts for methane activation.

For many reaction processes that require a catalyst, there is a desire to identify a quantifiable property that is easily measurable and can predict a suitable novel candidate to carry out the reaction of interest. An approach to such identification is known as a descriptor and has been investigated in detail for many catalysts and reactions.[84, 85, 130, 131] Examination of the catalyst properties (active oxygen vacancy, adsorption energy, activation energy) calculated in this work, shows that a linear relationship exists between the formation energy of the active vacancies and the adsorption energy of the dissociated species, shown in Figure 14. The graph shows that more favourable oxygen vacancy formation correlates to more favourable dissociative CH_4 adsorption. This existing relationship provides a strong platform to predict new materials for methane activation, as the reducibility of the surface can be related to the adsorption energy of the dissociation products. The oxygen vacancy formation energy of the material can therefore be used as a simple descriptor to predict the stability of the dissociated products, which in principle can be related to the activation energy by the Bronsted-Evans-Polyani relationship on catalytic surfaces.[132]

A decrease in adsorption energy from Mg to Ca doped CeO_2 is followed by a decrease in activation energy indicating the energy barrier is reduced with a lowering of the CH_3^* + H binding, however Sr doping does not follow this trend. Transition states were calculated for different combinations of $CH_3^{\cdot}$ + H on Sr-doped CeO_2 to examine if there is another transition state that can provide an activation energy that will follow the trend; however the reported transition state in this paper gives the lowest activation energy. There is thus no significant correlation observed for the adsorption energy of the dissociation products and the energy barrier for CH_4 activation for alkaline earth metal doped CeO_2 (111). This suggests that the relationship between these quantities is dopant dependant and may be difficult to correlate for metal oxide systems.

Conclusion

We present a density functional theory investigation of the activation of methane on alkaline earth metal doped (111) surface of CeO_2. Doping with alkaline earth metals requires the

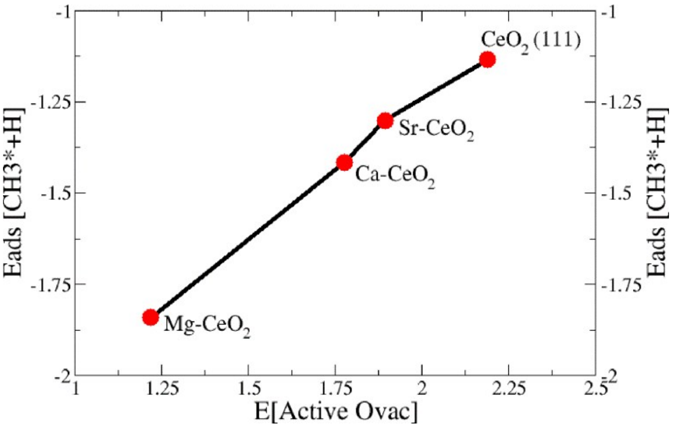

Figure 14: The correlation between the adsorption energy of the dissociation products and the formation energy of the active oxygen vacancy on the bare and doped (111) surfaces of CeO_2.

Catalysis Science & Technology Accepted Manuscript

This journal is © The Royal Society of Chemistry 20xx

inclusion of a charge compensating oxygen vacancy to correctly describe the ground state electronic structure of these surfaces. The removal of a second oxygen atom, that is the ‘active oxygen vacancy’, is used to assess the reducibility of the doped surface compared to the bare (111) surface. The active oxygen vacancy formation energy is seen to be lower than the formation of an oxygen vacancy at the bare surface, indicating that the doping of the surface promotes oxygen vacancy formation. The formation energy increases with increased ionic radius of alkaline earth metal dopants, so that the reducibility of the surface becomes more difficult as the dopant ionic radius increases.

The adsorption of CH_4 and its dissociation to $CH_3^{\cdot}$ + H was also investigated. The adsorption of CH_4 at all surfaces is weak, while the dissociation products show a large gain in energy upon interaction with the surface. The gain in energy is larger on the doped surfaces than the bare (111) surface of CeO_2, which indicates that doping enhances the dissociation of CH_4. The smaller Mg dopant has the strongest adsorption energy for the dissociation products which decreases with increasing ionic radius of the dopant. The calculated activation energies for C-H bond breaking on the Mg and Ca doped surfaces are lower than the bare surface, while the Sr doped surface has a larger activation energy suggesting it is worse than the bare surface. The Ca doped CeO_2 (111) surface has a lower activation barrier than Mg doped, which has been attributed to the stabilisation of the transition state by forming Ce-C bonds at the surface. This can occur from the Ca promotion of oxygen vacancies close to the dopant, which facilitates Ce-C bond formation, outlining the importance of charge compensating oxygen vacancies to correctly describe the ground state electronic structure for reactions on similar doped surfaces. From the calculated energies for active oxygen vacancy formation and adsorption of CH_3^* + H, a linear correlation is observed indicating that a relationship exists between the two quantities. This provides a simple descriptor to develop catalysts for methane activation as the reducibility of the catalyst material can predict the dissociation energy of the products, and hence the materials effectiveness for methane activation. We find no such relationship between the activation energy and the adsorption energy of the dissociation products for this particular set of dopants.

The calculated adsorption energies and activation energies suggest that for rational catalyst design in doping metal oxides for methane activation, three important properties must be considered;

1) Oxygen vacancy charge compensation: For further DFT studies, the change in the local geometric structure from the presence of the compensating oxygen vacancy can influence the stability of the transition state, and is required to correctly describes the reaction processes on the catalyst surface.

2) Ionic radius: The ionic radius of the dopant cation may play a role in determining the thermodynamics and the kinetics for methane activation on the doped surface. Dopants with smaller ionic radius than the host catalyst promote thermodynamics and kinetics over the bare catalyst surface, albeit a limit is reached when a dopant has a similar ionic radius to the host material. Selecting a dopant with a larger ionic radius than the host cation is seen to worsen both the thermodynamics and kinetics, suggesting this should be avoided. This can be further developed through studies of other sets of dopants with different ionic radii.

3) Reducibility: Oxygen vacancy formation can be used as a simple descriptor to ascertain activity for methane activation.

Acknowledgements

We acknowledge funding from the European FP7 NMP 2013 project BIOGO (grant no: 604296) *(Catalytic partial oxidation of biogas and reforming of pyrolysis oil for synthetic gas production and conversion into fuels,* www.biogo.eu). Computational resources are provided by the science foundation ireland (SFI) funded Irish Centre for High-end Computing (ICHEC), and by SFI funded resources at Tyndall.

Notes and references

1 P. Weiland, *Applied Microbiology and Biotechnology*, 2010, **85,** 849

2 J. B. Holm-Nielsen, T. Al Seadi and P. Oleskowicz-Popiel, *Bioresource Technology*, 2009, **100,** 5478

3 J. Dignon and S. Hameed, *JAPCA*, 1989, **39,** 180

4 M. Kampa and E. Castanas, *Environmental Pollution*, 2008, **151,** 362

5 N. Abatzoglou and S. Boivin, *Biofuels, Bioproducts and Biorefining*, 2009, **3,** 42

6 J. R. Rostrup-Nielsen, *Catalysis Today*, 2000, **63,** 159

7 U. Balachandran, J. T. Dusek, R. L. Mieville, R. B. Poeppel, M. S. Kleefisch, S. Pei, T. P. Kobylinski, C. A. Udovich and A. C. Bose, *Applied Catalysis A: General*, 1995, **133,** 19

8 Q. Miao, G. Xiong, S. Sheng, W. Cui, L. Xu and X. Guo, *Applied Catalysis A: General*, 1997, **154,** 17

9 V. R. Choudhary, A. M. Rajput and B. Prabhakar, *Catalysis Letters*, 1995, **32,** 391

10 V. R. Choudhary, B. S. Uphade and A. S. Mamman, *Catalysis Letters*, 1995, **32,** 387

11 R. A. Periana, D. J. Taube, E. R. Evitt, D. G. Löffler, P. R. Wentrcek, G. Voss and T. Masuda, *Science*, 1993, **259,** 340

12 H. D. Gesser, N. R. Hunter and C. B. Prakash, *Chemical Reviews*, 1985, **85,** 235

13 M. Muehlhofer, T. Strassner and W. A. Herrmann, *Angewandte Chemie International Edition*, 2002, **41,** 1745

14 N. R. Foster, *Applied Catalysis*, 1985, **19,** 1

Catalysis Science & Technology Accepted Manuscript

Please do not adjust margins

15 C. J. Jones, D. Taube, V. R. Ziatdinov, R. A. Periana, R. J. Nielsen, J. Oxgaard and W. A. Goddard, *Angewandte Chemie*, 2004, **116,** 4726

16 M. J. Brown and N. D. Parkyns, *Catalysis Today*, 1991, **8,** 305

17 T. J. Hall, J. S. J. Hargreaves, G. J. Hutchings, R. W. Joyner and S. H. Taylor, *Fuel Processing Technology*, 1995, **42,** 151

18 K. Otsuka and M. Hatano, *Journal of Catalysis*, 1987, **108,** 252

19 M. R. Smith and U. S. Ozkan, *Journal of Catalysis*, 1993, **141,** 124

20 R. G. Herman, Q. Sun, C. Shi, K. Klier, C.-B. Wang, H. Hu, I. E. Wachs and M. M. Bhasin, *Catalysis Today*, 1997, **37,** 1

21 R. A. Periana, O. Mironov, D. Taube, G. Bhalla and C. Jones, *Science*, 2003, **301,** 814

22 J. H. Lunsford, *Angewandte Chemie International Edition in English*, 1995, **34,** 970

23 V. Sadykov, N. Mezentseva, G. Alikina, R. Bunina, V. Pelipenko, A. Lukashevich, S. Tikhov, V. Usoltsev, Z. Vostrikov, O. Bobrenok, A. Smirnova, J. Ross, O. Smorygo and B. Rietveld, *Catalysis Today*, 2009, **146,** 132

24 S. J. Blanksby and G. B. Ellison, *Accounts of Chemical Research*, 2003, **36,** 255

25 J. H. Edwards and A. M. Maitra, *Fuel Processing Technology*, 1995, **42,** 269

26 S. Wang, G. Q. Lu and G. J. Millar, *Energy & Fuels*, 1996, **10,** 896

27 M. C. J. Bradford and M. A. Vannice, *Catalysis Reviews*, 1999, **41,** 1

28 L. Hanley, Z. Xu and J. T. Yates, *Surface Science*, 1991, **248,** L265

29 L. Juurlink, R. Smith, D. Killelea and A. Utz, *Physical Review Letters*, 2005, **94,** 208303

30 M. C. Bradford and M. A. Vannice, *Applied Catalysis A: General*, 1996, **142,** 97

31 P. Kratzer, B. Hammer and J. No, *The Journal of Chemical Physics*, 1996, **105,** 5595

32 J. D. Beckerle, A. D. Johnson, Q. Y. Yang and S. T. Ceyer, *The Journal of Chemical Physics*, 1989, **91,** 5756

33 L. B. F. Juurlink, R. R. Smith, D. R. Killelea and A. L. Utz, *Physical Review Letters*, 2005, **94,** 208303

34 A. C. Luntz and D. S. Bethune, *The Journal of Chemical Physics*, 1989, **90,** 1274

35 J. Harris, J. Simon, A. C. Luntz, C. B. Mullins and C. T. Rettner, *Physical Review Letters*, 1991, **67,** 652

36 M. Valden, N. Xiang, J. Pere and M. Pessa, *Applied Surface Science*, 1996, **99,** 83

37 V. A. Ukraintsev and I. Harrison, *The Journal of Chemical Physics*, 1994, **101,** 1564

38 K. M. DeWitt, L. Valadez, H. L. Abbott, K. W. Kolasinski and I. Harrison, *The Journal of Physical Chemistry B*, 2006, **110,** 6705

39 C.-T. Au, M.-S. Liao and C.-F. Ng, *The Journal of Physical Chemistry A*, 1998, **102,** 3959

40 G. Gajewski and C.-W. Pao, *The Journal of Chemical Physics*, 2011, **135,** 064707

41 Y.-H. Chin, C. Buda, M. Neurock and E. Iglesia, *Journal of the American Chemical Society*, 2013, **135,** 15425

42 A. Erdohelyi, J. Cserenyi and F. Solymosi, *Journal of Catalysis*, 1993, **141,** 287

43 T. P. Beebe, D. W. Goodman, B. D. Kay and J. T. Yates, *The Journal of Chemical Physics*, 1987, **87,** 2305

44 H. L. Abbott and I. Harrison, *The Journal of Physical Chemistry B*, 2005, **109,** 10371

45 C. N. Stewart and G. Ehrlich, *The Journal of Chemical Physics*, 1975, **62,** 4672

46 S. L. Tait, Z. Dohnálek, C. T. Campbell and B. D. Kay, *Surface Science*, 2005, **591,** 90

47 F. Abild-Pedersen, O. Lytken, J. Engbæk, G. Nielsen, I. Chorkendorff and J. K. Nørskov, *Surface Science*, 2005, **590,** 127

48 H. Ueta, L. Chen, R. D. Beck, I. Colon-Diaz and B. Jackson, *Physical Chemistry Chemical Physics*, 2013, **15,** 20526

49 P. W. van Grootel, R. A. van Santen and E. J. M. Hensen, *The Journal of Physical Chemistry C*, 2011, **115,** 13027

50 I. M. Ciobîcă, F. Frechard, R. A. van Santen, A. W. Kleyn and J. Hafner, *The Journal of Physical Chemistry B*, 2000, **104,** 3364

51 Y.-Z. Lin, J. Sun, J. Yi, J.-D. Lin, H.-B. Chen and D.-W. Liao, *Journal of Molecular Structure: THEOCHEM*, 2002, **587,** 63

52 M. C. J. Bradford and M. A. Vannice, *Catalysis Letters*, 1997, **48,** 31

53 J. Wei and E. Iglesia, *The Journal of Physical Chemistry B*, 2004, **108,** 4094

54 F. Solymosi, A. Erdöhelyi and J. Cserényi, *Catalysis Letters*, 1992, **16,** 399

55 C.-Q. Lv, K.-C. Ling and G.-C. Wang, *The Journal of Chemical Physics*, 2009, **131,** 144704

56 A. Trovarelli, *Catalysis Reviews*, 1996, **38,** 439

57 R. Fiorenza, C. Crisafulli, G. G. Condorelli, F. Lupo and S. Scirè, *Catalysis Letters*, 2015, **145,** 1691

58 S. Xiong, Y. Liao, X. Xiao, H. Dang and S. Yang, *The Journal of Physical Chemistry C*, 2015, **119,** 4180

59 J. Quiroz, J.-M. Giraudon, A. Gervasini, C. Dujardin, C. Lancelot, M. Trentesaux and J.-F. Lamonier, *ACS Catalysis*, 2015, **5,** 2260

60 P. Fornasiero, R. Dimonte, G. R. Rao, J. Kaspar, S. Meriani, A.-. Trovarelli and M. Graziani, *Journal of Catalysis*, 1995, **151,** 168

61 Q. Fu, A. Weber and M. Flytzani-Stephanopoulos, *Catalysis Letters*, 2001, **77,** 87

62 J. Guzman, S. Carrettin and A. Corma, *Journal of the American Chemical Society*, 2005, **127,** 3286

63 S.-I. Lee, J. M. Vohs and R. J. Gorte, *Journal of the Electrochemical Society*, 2004, **151,** A1319

64 H. He, J. M. Vohs and R. J. Gorte, *Journal of the Electrochemical Society*, 2003, **150,** A1470

65 K. Ahn, H. He, J. M. Vohs and R. J. Gorte, *Electrochemical and Solid-State Letters*, 2005, **8,** A414

66 B. Rambabu, S. Ghosh and H. Jena, *Journal of materials science*, 2006, **41,** 7530

67 T. Mori and H. Yamamura, *Journal of Materials Synthesis and Processing*, 1998, **6,** 175

68 Q. Li and V. Thangadurai, *Fuel Cells*, 2009, **9,** 684

69 I. Yeriskin and M. Nolan, *Journal of Chemical Physics*, 2009, **131,** 244702

70 C. Kleinlogel and L. J. Gauckler, *Advanced Materials*, 2001, **13,** 1081

71 K. Singh, S. Acharya and S. Bhoga, *Ionics*, 2007, **13,** 429

72 E. Ruiz-Trejo, A. Benitez-Rico, S. Gomez-Reynoso and M. Angeles-Rosas, *Journal of the Electrochemical Society*, 2007, **154,** A258

73 J.-G. Duh, H.-T. Dai and W.-Y. Hsu, *Journal of materials science*, 1988, **23,** 2786

74 J. Nunan, W. Williamson and H. Robota, *Journal*, 1996,

75 E. Rohart, S. Verdier, A. Demourgues, V. Harlé, B. Pacaud, A. Baylet, H. Takemori, E. Suda and M. Allain, *Journal*, 2006,

76 Y. Hirasawa, K. Katoh, T. Yamada and A. Kohara, *Journal*, 2009,

77 Y.-K. Lui and J. C. Dettling, *Journal*, 1993,

78 Z. Zhan, X. Liu, D. Ma, L. Song, J. Li, H. He and H. Dai, *Frontiers of Environmental Science & Engineering*, 2014, **8,** 483

79 M. Nolan and G. W. Watson, *The Journal of Physical Chemistry B*, 2006, **110,** 16600

Catalysis Science & Technology Accepted Manuscript

This journal is © The Royal Society of Chemistry 20xx

80 M. Nolan, S. C. Parker and G. W. Watson, *The Journal of Physical Chemistry B*, 2006, **110,** 2256

81 D. C. Sayle, S. A. Maicaneanu and G. W. Watson, *Journal of the American Chemical Society*, 2002, **124,** 11429

82 M. Nolan, S. Grigoleit, D. C. Sayle, S. C. Parker and G. W. Watson, *Surface Science*, 2005, **576,** 217

83 M. V. Ganduglia-Pirovano, J. L. F. Da Silva and J. Sauer, *Physical Review Letters*, 2009, **102,** 026101

84 V. Botu, R. Ramprasad and A. B. Mhadeshwar, *Surface Science*, 2014, **619,** 49

85 M. V. Ganduglia-Pirovano, C. Popa, J. Sauer, H. Abbott, A. Uhl, M. Baron, D. Stacchiola, O. Bondarchuk, S. Shaikhutdinov and H.-J. Freund, *Journal of the American Chemical Society*, 2010, **132,** 2345

86 M. Nolan, S. C. Parker and G. W. Watson, *Physical Chemistry Chemical Physics*, 2006, **8,** 216

87 D. O. Scanlon, N. M. Galea, B. J. Morgan and G. W. Watson, *The Journal of Physical Chemistry C*, 2009, **113,** 11095

88 J. Harmsen, J. Hoebink and J. Schouten, *Catalysis Letters*, 2001, **71,** 81

89 M. Nolan, *The Journal of Chemical Physics*, 2009, **130,** 144702

90 M. B. Watkins, A. S. Foster and A. L. Shluger, *The Journal of Physical Chemistry C*, 2007, **111,** 15337

91 Z. Lu, C. Müller, Z. Yang, K. Hermansson and J. Kullgren, *The Journal of Chemical Physics*, 2011, **134,** 184703

92 G. S. Wong, M. R. Concepcion and J. M. Vohs, *The Journal of Physical Chemistry B*, 2002, **106,** 6451

93 W. Daniell, A. Ponchel, S. Kuba, F. Anderle, T. Weingand, D. Gregory and H. Knözinger, *Topics in Catalysis*, 2002, **20,** 65

94 W. Zhang, X. Zhou, D. Tang, H. Wan and K. Tsai, *Catalysis Letters*, 1994, **23,** 103

95 H. Y. Kim and G. Henkelman, *The Journal of Physical Chemistry Letters*, 2012, **4,** 216

96 H.-S. Roh, K.-W. Jun, S.-C. Baek and S.-E. Park, *Chemistry Letters*, 2001, **30,** 1048

97 K. Otsuka, Y. Wang, E. Sunada and I. Yamanaka, *Journal of Catalysis*, 1998, **175,** 152

98 A. P. York, T. Xiao and M. L. Green, *Topics in Catalysis*, 2003, **22,** 345

99 D. Knapp and T. Ziegler, *The Journal of Physical Chemistry C*, 2008, **112,** 17311

100 A. D. Mayernick and M. J. Janik, *The Journal of Physical Chemistry C*, 2008, **112,** 14955

101 V. J. Ferreira, P. Tavares, J. L. Figueiredo and J. L. Faria, *Industrial & Engineering Chemistry Research*, 2012, **51,** 10535

102 M. Nolan, Y. Lykhach, N. Tsud, T. Skála, T. Staudt, K. C. Prince, V. Matolín and J. Libuda, *Physical Chemistry Chemical Physics*, 2012, **14,** 1293

103 A. B. Kehoe, D. O. Scanlon and G. W. Watson, *Chemistry of Materials*, 2011, **23,** 4464

104 M. D. Krcha, A. D. Mayernick and M. J. Janik, *Journal of Catalysis*, 2012, **293,** 103

105 G. Henkelman, B. P. Uberuaga and H. Jónsson, *The Journal of Chemical Physics*, 2000, **113,** 9901

106 D. Sheppard, R. Terrell and G. Henkelman, *The Journal of Chemical Physics*, 2008, **128,** 134106

107 G. Henkelman, G. Jóhannesson and H. Jónsson, *Theoretical Methods in Condensed Phase Chemistry*, 2002, 269

108 D. Sheppard, P. Xiao, W. Chemelewski, D. D. Johnson and G. Henkelman, *The Journal of Chemical Physics*, 2012, **136,** 074103

109 J. P. Perdew, K. Burke and M. Ernzerhof, *Physical Review Letters*, 1996, **77,** 3865

110 G. Kresse and J. Furthmüller, *Computational Materials Science*, 1996, **6,** 15

111 G. Kresse and J. Furthmüller, *Physical Review B*, 1996, **54,** 11169

112 G. Kresse, *Physical Review B: Condensed Matter*, 1996, **54,** 11

113 G. Kresse and J. Furthmüller, *Physical Review B: Condensed Matter*, 1996, **54,** 169

114 G. Kresse and D. Joubert, *Physical Review B*, 1999, **59,** 1758

115 S. Dudarev, G. Botton, S. Savrasov, C. Humphreys and A. Sutton, *Physical Review B*, 1998, **57,** 1505

116 O. Bengone, M. Alouani, P. Blöchl and J. Hugel, *Physical Review B*, 2000, **62,** 16392

117 M. Nolan, J. E. Fearon and G. W. Watson, *Solid State Ionics*, 2006, **177,** 3069

118 M. Nolan, S. C. Parker and G. W. Watson, *Surface Science*, 2005, **595,** 223

119 H. J. Monkhorst and J. D. Pack, *Physical Review B*, 1976, **13,** 5188

120 F. Murnaghan, *Proceedings of the national academy of sciences of the United States of America*, 1944, **30,** 244

121 A. Sundaresan, R. Bhargavi, N. Rangarajan, U. Siddesh and C. N. R. Rao, *Physical Review B*, 2006, **74,** 161306

122 G. Henkelman, A. Arnaldsson and H. Jónsson, *Computational Materials Science*, 2006, **36,** 354

123 W. Tang, E. Sanville and G. Henkelman, *Journal of Physics: Condensed Matter*, 2009, **21,** 084204

124 E. Sanville, S. D. Kenny, R. Smith and G. Henkelman, *Journal of computational chemistry*, 2007, **28,** 899

125 Y. Pan, N. Nilius, H.-J. Freund, J. Paier, C. Penschke and J. Sauer, *Physical Review Letters*, 2013, **111,** 206101

126 G. E. Murgida and M. V. Ganduglia-Pirovano, *Physical Review Letters*, 2013, **110,** 246101

127 S. P. Mehandru, A. B. Anderson and J. F. Brazdil, *Journal of the American Chemical Society*, 1988, **110,** 1715

128 H. Metiu, S. Chrétien, Z. Hu, B. Li and X. Sun, *The Journal of Physical Chemistry C*, 2012, **116,** 10439

129 E. W. McFarland and H. Metiu, *Chemical Reviews*, 2013, **113,** 4391

130 A. A. Peterson and J. K. Nørskov, *The Journal of Physical Chemistry Letters*, 2012, **3,** 251

131 J. K. Nørskov, F. Abild-Pedersen, F. Studt and T. Bligaard, *Proceedings of the National Academy of Sciences*, 2011, **108,** 937

132 R. A. v. Santen, M. Neurock and S. G. Shetty, *Chemical Reviews*, 2009, **110,** 2005

Catalysis Science & Technology Accepted Manuscript

Please do not adjust margins

Table of contents figure

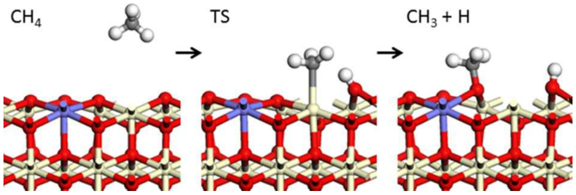

Alkaline earth metal doping of CeO_2 improves the dissociative adsorption of methane with the behaviour showing a correlation to dopant ionic radius

Catalysis Science & Technology Accepted Manuscript